Two-Body Contact Dynamics in a Bose Gas near a Fano-Feshbach Resonance

Alexandre Journeaux,[1] Julie Veschambre,[1] Maxime Lecomte,[1] Ethan Uzan,[1] Jean Dalibard,[1] Félix Werner,[1] Dmitry S. Petrov,[2] and Raphael Lopes[1,*]

[1]*Laboratoire Kastler Brossel, Collège de France, CNRS, ENS-Université PSL, Sorbonne Université, 11 Place Marcelin Berthelot, 75005 Paris, France*

[2]*Université Paris-Saclay, CNRS, LPTMS, 91405 Orsay, France*

(Received 19 September 2025; revised 2 January 2026; accepted 26 January 2026; published 26 February 2026)

We investigate the real-time buildup of short-range correlations in a nondegenerate ultracold Bose gas near a narrow Fano-Feshbach resonance. Using rapid optical control, we quench the closed-channel molecular energy to resonance on submicrosecond timescales and track the evolution of the two-body contact through photodissociation losses. Repeated pulse sequences enhance sensitivity to early-time two-body losses and reveal long-lived coherence between atom pairs and molecular states. The observed dynamics are accurately reproduced by our dynamical two-channel zero-range theory, which explicitly accounts for the resonance's narrow width and finite closed-channel decay, establishing a predictive framework for correlation dynamics in quantum gases near Fano-Feshbach resonances.

DOI: 10.1103/prf8-3q27

Understanding and predicting out-of-equilibrium dynamics in quantum many-body systems is one of the central challenges of modern physics. Ultracold gases offer a pristine test bed to address this challenge, with well-defined initial states, tunable interactions, and microscopic dynamics that can be resolved directly in experiment. This unique level of control has enabled landmark observations of nonequilibrium phenomena in quantum gases [1–9].

Among the various nonequilibrium settings explored so far, a paradigmatic case is the three-dimensional Bose gas quenched from the weakly interacting regime to the maximally interacting unitary limit, whose experimental study [10–15] stimulated extensive theoretical activity [16–30]. The dynamics of this system are governed by the buildup of short-range two-body correlations, which are naturally described in terms of Tan's contact $\mathcal{C}_2$ [31–38], a unifying concept in quantum gases with close connections to nuclear physics [39–42]. The contact $\mathcal{C}_2$, proportional to the probability of finding two atoms at short interparticle distances, connects microscopic and thermodynamic quantities through exact relations. While $\mathcal{C}_2$ has been measured at equilibrium [11,43,44], its nonequilibrium dynamics remain elusive [10,14], most likely because of additional three-body contributions [28,45].

A natural probe of $\mathcal{C}_2$ is provided by microscopic loss mechanisms, such as photodissociation of closed-channel molecules, which have long served as sensitive diagnostics of short-range correlations at equilibrium [46–49]. These processes directly reflect the amplitude of short-range correlations while minimally perturbing the many-body state, making them a promising route to probe correlation dynamics in real time. However, exploiting them to follow the growth of correlations requires interaction control on timescales shorter than the buildup time, which remains a significant experimental challenge.

Probing the dynamics of $\mathcal{C}_2$ can be carried out near both broad and narrow Fano-Feshbach resonances (FFRs). While broad resonances are fully characterized by the scattering length [50], narrow resonances enrich this description by introducing an additional length scale $R^\star$ set by the effective range and inversely proportional to the resonance width [51–53]. This distinctive feature makes them a powerful platform to explore effective-range effects, which are of central importance in low-energy nuclear systems [54–56].

In this Letter, we implement a new approach based on optical tuning of the closed-channel molecular state, enabling genuine sudden quenches on submicrosecond timescales and providing access to previously unresolved contact dynamics. This fast control is achieved via spin-dependent light shifts arising from the large vectorial and tensorial polarizability of lanthanide atoms [57–60]. By periodically cycling between resonant and weak interactions, we enhance sensitivity to early-time two-body losses and resolve the buildup of short-range correlations following an interaction quench. We develop a two-channel model that incorporates the narrow resonance width and molecular-state dissipation, relates the two-body loss rate to the instantaneous contact $\mathcal{C}_2(t)$, and accurately reproduces the observed dynamics. Finally, by varying the off-resonant time, we observe oscillations of the two-body loss rate, extending previous observations of interference effects

*Contact author: raphael.lopes@lkb.ens.fr

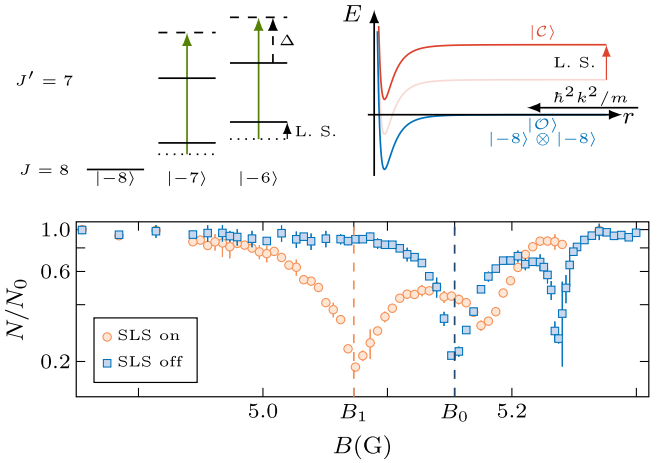

FIG. 1. Fano-Feshbach resonance displacement induced by a spin-dependent light shift. Top: illustration of the coupling between the ground-state manifold with total angular momentum $J = 8$ and the excited-state manifold associated with the transition at wavelength $\lambda = 530.306$ nm, with $J' = 7$. This coupling induces a light shift that displaces the energy of the closed-channel molecular state $|\mathcal{C}\rangle$, while the open-channel collisional state $|\mathcal{O}\rangle$ remains unaffected. Bottom: loss features in the presence (disks) and absence (squares) of the spin-dependent light shift (SLS) laser, showing the optical displacement of the magnetic Fano-Feshbach resonance from B_0 to B_1 for a thermal sample of ^{162}Dy with $N = 3 \times 10^4$ atoms and temperature $T = 1.24$ μK. In the "SLS on" (resp. "SLS off") case we hold the sample for 15 ms (resp. 150 ms).

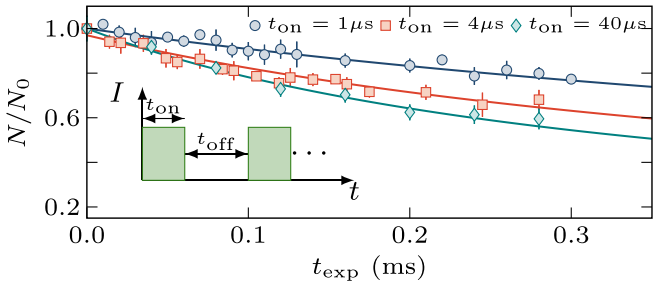

FIG. 2. Probing two-body loss dynamics. Atom number as a function of exposure time, $t_{\rm exp} = t_{\rm on} N_{\rm cycles}$, for three different values of $t_{\rm on}$ (see legend), at a temperature $T = 0.34$ μK, and initial atom number $N_0 \approx 2 \times 10^4$. Here, $t_{\rm off} = 26$ μs. Solid lines are fits using Eq. (1). Inset: schematic of the pulsing protocol.

arising from the coherent superposition of dimer and unbound atomic states [61–63].

We perform the experiment with ^{162}Dy atoms and use a laser beam detuned by $\Delta = 2\pi \times 20$ GHz from the optical transition at $\lambda = 530.306$ nm, which couples the ground-state manifold with total angular momentum $J = 8$ to an excited state with $J' = J - 1$ [64] (see Fig. 1). This beam is linearly polarized along $\hat{z}$, resulting in a light shift for most closed-channel molecular states [65,66]. By contrast, the open-channel state, composed of atoms in the spin configuration $|-8\rangle \otimes |-8\rangle$, remains effectively decoupled from the light field. As a result, we do not observe heating or atom loss due to spontaneous emission when operating far from the FFR.

This spin-dependent light shift (SLS) leads to a displacement of the FFR pole from its original position B_0 to a new magnetic field B_1. The shift is given by $B_1 - B_0 \propto -I/(\Delta\delta\mu)$, where I is the laser intensity and $\delta\mu > 0$ the differential magnetic moment between the molecular and atomic states.

Our experiments start with a thermal sample of typically 10^5 atoms. As shown in Fig. 1, the SLS beam shifts the FFR loss feature from $B_0 \approx 5.15$ G to $B_1 \approx 5.07$ G. This shift enables a rapid change in scattering length, from $a \approx 140\ a_0$ to resonance ($a \to \infty$), within 200 ns [2,67]. In addition to shifting the resonance, the laser also induces two-body losses due to photodissociation of closed-channel molecules, which we use here as a tool for probing short-range correlations. The laser-induced energy shift of the closed-channel molecule and the associated two-body loss thus provide a method to probe the dynamics of short-range two-body correlations.

To better resolve the dynamics we employ a repeated pulsing protocol that improves the detectability of two-body losses by accumulating their effects over many interaction quenches near resonance (see Fig. 2 inset). This approach enhances sensitivity to small loss rates without modifying the underlying inelastic mechanism. Specifically, we prepare a thermal gas at the magnetic field B_1, and apply a sequence of optical pulses: the SLS beam is turned on for a duration $t_{\rm on}$, followed by an off period $t_{\rm off}$ long enough to ensure that successive pulses act independently. This sequence is repeated $N_{\rm cycles}$ times, resulting in a total exposure time $t_{\rm exp} = t_{\rm on} N_{\rm cycles}$ [69].

In Fig. 2, we show the atom number evolution as a function of $t_{\rm exp}$ for a thermal sample with temperature $T = 0.34(1)$ μK and three values of $t_{\rm on}$ with $t_{\rm off} = 26$ μs. For a fixed $t_{\rm exp}$, we observe a monotonic increase in atom loss with increasing $t_{\rm on}$, a signature that the two-body loss rate is dynamically evolving. We fit the data using a two-body loss model,

$$\frac{dN}{dt_{\rm exp}} = -L_2(t_{\rm on}, t_{\rm off})\bar{n}N, \tag{1}$$

where $\bar{n} = n_0/\sqrt{8}$ is the spatially averaged density, assuming a Gaussian spatial distribution with peak value n_0. We extract the effective two-body loss coefficient $L_2(t_{\rm on}, t_{\rm off})$, defined as

$$L_2(t_{\rm on}, t_{\rm off}) = \frac{1}{t_{\rm exp}} \int_0^{(t_{\rm on}+t_{\rm off})N_{\rm cycles}} \mathcal{L}_2(t)dt, \tag{2}$$

where $\mathcal{L}_2$ is the instantaneous loss rate such that locally $\dot{n} = -\mathcal{L}_2 n^2$. The right-hand side of Eq. (2) would be

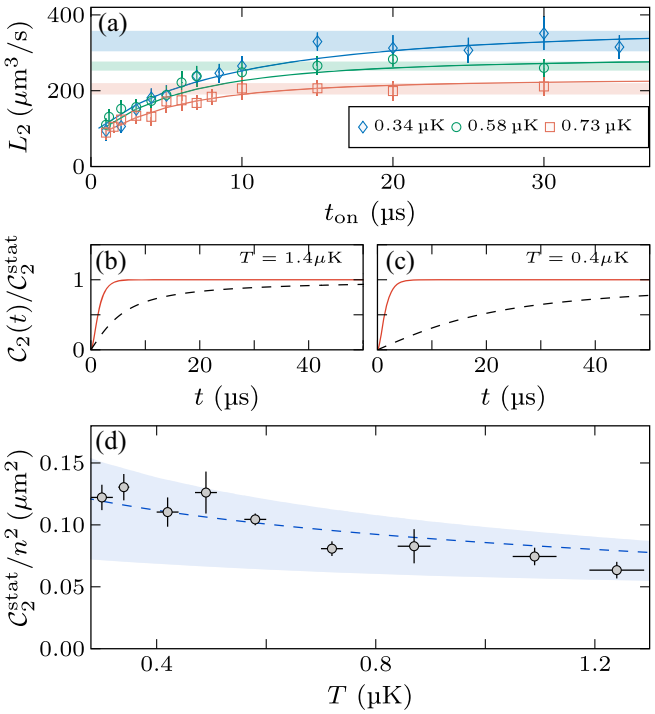

FIG. 3. Two-body contact dynamics. (a) Measured two-body loss coefficient L_2 for different temperatures (see legends). Solid lines are fits using Eq. (4). The shaded region indicates the value of $\bar{L}_2$ plus or minus one standard deviation. (b) Evolution of $\mathcal{C}_2(t)$, scaled by its stationary value, for $R^\star \to 0$ and $\Gamma_b = 0$ (black dashed line), $R^\star \to \infty$ and $\Gamma_b/2\pi = 300$ kHz (red line), for a thermal sample at 1.4 μK. (c) Same comparison for a thermal sample at 0.4 μK. (d) Temperature dependence of $\mathcal{C}_2^{stat}/n^2$, deduced from $\bar{L}_2$, and compared with the theoretical prediction from Eq. (5). The blue dashed line shows the prediction from Eq. (5), with the values of $R^\star$ and Γ_b^{on} given by Eq. (7) and the corresponding error bars reflected by the shaded area.

independent of both t_{on} and t_{off} if $\mathcal{L}_2$ was constant during t_{on} and zero during t_{off}. Accordingly, L_2 allows us to quantify deviations from this simple scenario. Since atom loss is accompanied by heating, we restrict our fit to data where the temperature increase is below 15% and take into account the small resulting change in effective volume due to thermal expansion of the cloud [69].

As shown in Fig. 3(a), for $t_{off} = 26$ μs, L_2 increases with t_{on} at short times and saturates for $t_{on} \gtrsim 20$ μs to an asymptotic value L_2^{stat}. We independently confirm this saturation behavior using a continuous-probe configuration, where $\bar{L}_2 = L_2(t_{off} = 0)$, shown as the shaded region in Fig. 3(a). The measured value of $\bar{L}_2$ agrees with L_2^{stat} within experimental uncertainty, reinforcing our interpretation that the pulsed sequence faithfully captures the buildup dynamics of two-body losses.

To model the observed dynamics, we reduce the many-body problem to a two-body problem, which can be justified in the nondegenerate regime by a virial expansion [22], and we adopt a zero-range two-channel description. In this framework, the wave function of the relative motion in the open channel $\Psi(\mathbf{r}, t)$ is coupled to the closed-channel amplitude $\phi(t)$, with coupling strength characterized by the range parameter $R^\star > 0$. We find that ϕ is related to the $1/r$ singularity of Ψ by the equation $\phi(t) = \sqrt{4\pi R^\star}\lim_{r\to 0} r\,\Psi(\mathbf{r}, t)$. As a consequence, the two-body contact is proportional to the density n_b of closed-channel molecules, $\mathcal{C}_2(t) = (8\pi/R^\star)n_b(t)$, a result previously established at equilibrium [47,72,73]. Since $n_b(t)$ equals $n^2/2$ times the thermal average $\langle|\phi(t)|^2\rangle_T$, and with each molecule being lost at a rate $\Gamma_b(t)$, the instantaneous atom loss rate constant is [74]

$$\mathcal{L}_2(t) = \Gamma_b(t)\,\frac{R^\star}{4\pi}\,\frac{\mathcal{C}_2(t)}{n^2} = \Gamma_b(t)\,\langle|\phi(t)|^2\rangle_T. \tag{3}$$

The problem of calculating the loss rate thus reduces to determining $\phi(t)$ for a pair of particles in a unit volume. We find (see Ref. [69]) that the evolution of $\phi(t)$ for two identical bosons with nonzero relative momentum k is governed by

$$i\hbar\dot{\phi}\,(t) - E_0(t)\phi(t) - \frac{\hbar^{3/2}}{\sqrt{i\pi m}R^\star}\int_{-\infty}^{t}\frac{\dot{\phi}(t')\mathrm{d}t'}{\sqrt{t-t'}} = -\frac{\hbar^2}{m}\sqrt{\frac{8\pi}{R^\star}}e^{-i\frac{\hbar k^2}{m}t}, \tag{4}$$

where $E_0(t) = -\hbar^2/[ma'(t)R^\star] - i\hbar\Gamma_b(t)/2$ is the complex closed-channel molecular energy detuning, and $1/a'(t)$ is the real part of the inverse scattering length.

In the stationary regime, substituting $\phi(t) = \phi^{stat}e^{-i\hbar k^2 t/m}$ into Eq. (4) yields an algebraic equation, whose solution gives the stationary contact density

$$\mathcal{C}_2^{stat} = n^2\lambda_T{}^2\int_0^\infty \mathrm{d}x\,\frac{32\sqrt{2}x^2e^{-x^2/(2\pi)}}{(\lambda_T/a' + x^2R^\star/\lambda_T)^2 + \left(\frac{m}{2\hbar}\Gamma_b\lambda_T R^\star + x\right)^2}, \tag{5}$$

where $\lambda_T = \sqrt{2\pi\hbar^2/(mk_BT)}$ is the thermal de Broglie wavelength. Equation (5) shows that $\mathcal{C}_2^{stat}$ depends on three dimensionless parameters characterizing, respectively, the dimer detuning, the resonance width, and the loss strength. For a broad lossless resonance ($R^\star \to 0, \Gamma_b \to 0$), $\mathcal{C}_2^{stat}$ becomes independent of the sign of a' and peaks at the resonance position, where we recover the universal result $\mathcal{C}_2^{stat} = 32\pi n^2\lambda_T{}^2$ [45]. By contrast, near a narrow resonance, the maximum of $\mathcal{C}_2^{stat}$ (and hence of L_2^{stat}) shifts to a finite negative scattering length ($\lambda_T/a' < 0$) [69].

When a' and Γ_b are suddenly quenched, the field ϕ evolves toward a new stationary state. As one can see from Eq. (4), the dynamics and associated timescales depend on

several parameters. For a single quench at $t = 0$ from a very large initial detuning to a value E_0 close to resonance we can neglect $\phi(t)$ at $t < 0$ and solve Eq. (4) analytically by the Laplace transform technique. One can check that the transform of $\phi(t)$ explicitly reads

$$\phi(s) = \frac{\sqrt{8\pi/R^\star}}{(k^2 - ims/\hbar)(s + iE_0/\hbar + \sqrt{i\hbar s/m}/R^\star)}. \quad (6)$$

The corresponding inverse Laplace transform is in general a bulky but analytic expression written in terms of error functions. It depends on the dimensionless parameters $mE_0/\hbar^2k^2$ (which is complex) and $kR^\star$, and we can choose, for example, $m/\hbar k^2$ as the overall timescale. For thermally averaged quantities we use the same parameter space with $m/\hbar k^2$ replaced by $\tau_T = \hbar/k_B T$. Let us discuss the dynamics after a quench to resonance, i.e., $\mathrm{Re}(E_0) = 0$, in two opposite limits described by compact formulas.

In the lossless ($\Gamma_b \ll 1/\tau_T$), broad-resonance ($R^\star \ll \lambda_T$) limit, we can neglect the first two terms in Eq. (4), or the corresponding terms in Eq. (6), and arrive at $(4\pi/R^\star)|\phi(t)|^2 = 32\pi^2|\mathrm{Erf}\sqrt{-i\hbar k^2 t/m}|^2/k^2$, where Erf is the error function. This quantity oscillates in time, but averaging over momenta leads to $\mathcal{C}_2(t) = 64n^2\lambda_T{}^2 \arctan(t/\tau_T)$ [27].

As a second example, we consider the lossy ($\Gamma_b \gg 1/\tau_T$), narrow-resonance limit ($R^\star \gg \lambda_T$), where we can neglect the integral term in Eq. (4). Then, $\phi(t) = i\sqrt{8\pi/R^\star}(e^{-i\hbar k^2 t/m} - e^{-\Gamma_b t/2})/(m\Gamma_b/2\hbar - ik^2)$ and, after thermal averaging, we obtain $\mathcal{C}_2(t) = (1 - e^{-\Gamma_b t/2})^2\, \mathcal{C}_2^{\mathrm{stat}}$. We note that, in this case, $\mathcal{C}_2(t) \propto t^2$ at short times [25], different from the $\mathcal{C}_2(t) \propto t$ scaling in the broad-resonance case [17,18,24,27]. In Figs. 3(b) and 3(c) we present a few examples of the time dependence of the contact density predicted for various experimental parameters following a single quench to resonance.

Using the periodic pulse protocol, we now experimentally and theoretically reveal the dynamics of the two-body contact. We examine the temperature dependence of the two-body loss rate dynamics by probing thermal samples from 0.30 to 1.24 μK. These temperatures are low enough to avoid contamination from nearby higher-partial-wave FFRs [75] while remaining high enough to ensure nondegenerate samples. We fit the data, treating $R^\star$ and Γ_b as adjustable parameters, with a Floquet-based numerical approach that solves Eq. (4) with periodic $E_0(t)$ and deduces L_2 from Eqs. (2) and (3) [69,76]. The model reproduces the measurements across the entire temperature range; see Fig. 3(a). From the fits we extract the on-resonance decay rate of the closed-channel molecule Γ_b^{on} and the range parameter $R^\star$, which are both nearly temperature independent and given by [69]

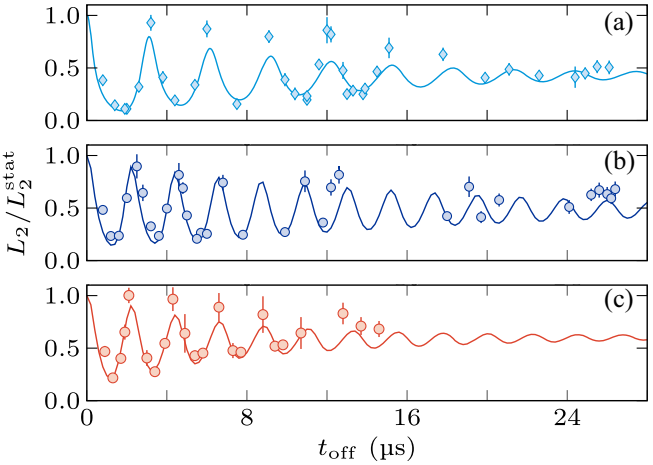

FIG. 4. Coherent oscillations of the two-body loss rate. Normalized loss rate L_2/L_2^{stat} as a function of t_{off} for a fixed $t_{\mathrm{on}} = 3$ μs. The solid line corresponds to numerical solutions of Eq. (4) using the parameters from Eq. (7). The values of $(T, \mathrm{Re}(E_0^{\mathrm{off}})/h)$ are (0.41 μK, −436 kHz) for (a), (0.41 μK, −560 kHz) for (b), and (1.24 μK, −560 kHz) for (c).

$$\Gamma_b^{\mathrm{on}}/(2\pi) = 123(38)\,\mathrm{kHz} \quad \text{and} \quad R^\star = 10.0(2.3)\ell_{\mathrm{vdW}}, \quad (7)$$

where $\ell_{\mathrm{vdW}} = 4.12$ nm is the van der Waals length [77]. As an independent check we perform bound-state spectroscopy, which yields $\Gamma_b^{\mathrm{on}}/2\pi = 112(30)$ kHz and $R^\star = 10.8(2.1)\ell_{\mathrm{vdW}}$, consistent with Eq. (7), as well as the values of the differential magnetic moment $\delta\mu = 4.15(18)\mu_B$ and the FFR position B_{res}, such that $\mathrm{Re}(E_0) = \delta\mu(B - B_{\mathrm{res}})$ (see End Matter).

We show in Fig. 3(d) the two-body contact density $\mathcal{C}_2^{\mathrm{stat}}/n^2$, deduced from $\bar{L}_2$ using Eq. (3), as a function of temperature. The measurements are well reproduced by Eq. (5) (dashed blue line), evaluated with the parameters from Eq. (7); the shaded band reflects the uncertainties in these parameters. These findings demonstrate a high degree of control over the observed two-body losses and establish their direct connection to the two-body contact density, whose dynamical evolution we resolve [69].

Finally, we study the dependence of $L_2(t_{\mathrm{on}}, t_{\mathrm{off}})$ on t_{off} at fixed $t_{\mathrm{on}} = 3$ μs. The data, shown in Fig. 4, reveal oscillations of the two-body loss rate, normalized by the asymptotic value L_2^{stat}. We attribute these oscillations to the fact that, between pulses, the system is quenched out of resonance to the negative $\mathrm{Re}(E_0^{\mathrm{off}})$ side, where the closed-channel molecular state lies far below the open-channel threshold and is thus protected from dissociation. During this period, the closed-channel amplitude acquires a phase factor $\approx e^{-iE_0^{\mathrm{off}} t_{\mathrm{off}}/\hbar}$, interfering with the open-channel component, which accumulates a phase $\approx e^{-i\hbar k^2 t_{\mathrm{off}}/m}$. The loss of contrast arises from thermal averaging over k and from the finite closed-channel decay rate Γ_b^{off}, which remains relatively small in our case (see End Matter).

Similar oscillations have been observed in double-pulse experiments [61–63]. A distinguishing feature of our experiment is the use of a periodic sequence of pulses. As shown in Fig. 4(a), the resulting oscillations deviate markedly from a simple sinusoid, exhibiting an extended minimum followed by a sharp, asymmetric peak. This waveform reflects interference between multiple pathways for molecule formation, each associated with one of the N_{cycle} on-resonant pulses.

To gain a more quantitative insight on these oscillations we numerically solve Eq. (4). The theory curve shown in Fig. 4(a) fits the data for a detuning $\mathrm{Re}(E_0^{\mathrm{off}})/h = -436(7)$ kHz, in good agreement with the expected detuning at the field B_1, $\mathrm{Re}(E_0^{\mathrm{off}})/h = \delta\mu(B_1 - B_0) = -470(40)$ kHz for the parameters determined in the End Matter. We then increase the SLS intensity by 40%, shifting the resonance pole to a lower magnetic field, $B_2 < B_1$, such that the off-resonant dimer energy is $\approx -h \times 560$ kHz. As a result, we observe faster oscillations, as shown in Fig. 4(b), confirming that the oscillation frequency is set by the off-resonant dimer energy.

As we have mentioned, the reduction of contrast with increasing t_{off} is attributed to the finite temperature of the gas and to the intrinsic loss rate of the off-resonant molecular state, quantified by $\Gamma_{\mathrm{b}}^{\mathrm{off}}$ (see End Matter). To check this, we repeat the measurement at a higher temperature, $T = 1.24$ μK. As shown in Fig. 4(c), the contrast decays more rapidly, as predicted by the numerical model, confirming that it is the thermal decoherence that plays the key role in the observed damping.

In conclusion, we achieve a direct measurement of the real-time buildup of two-body correlations in a thermal Bose gas near a narrow resonance, enabled by submicrosecond interaction quenches. By connecting the temporal evolution of the two-body loss rate to Tan's contact, we establish controlled dissipation as a powerful probe of short-range correlations, extending earlier studies of strongly interacting gases at equilibrium into the dynamical regime. The excellent agreement with a two-channel model demonstrates its predictive capacity and paves the way for exploring new quench protocols, pulse sequences, and interaction regimes. Looking ahead, the experimental and theoretical advances demonstrated here open promising routes to probe the nonequilibrium dynamics of Tan's contact in degenerate Bose gases, including the most challenging strongly correlated regime.

Acknowledgments—We acknowledge fruitful discussions with Z. Hadzibabic and the members of the Bose-Einstein condensate team at LKB. This research was funded, in part, by Agence Nationale de la Recherche (ANR), Projects No. ANR-20-CE30-0024, No. ANR-24-CE30-7961, and No. ANR-21-CE30-0033. This work was also funded by Region Ile-de-France in the framework of DIM QuanTiP, and supported by a grant from the "Fondation CFM pour la Recherche."

Data availability—The data that support the findings of this article are openly available [78].

[1] M. Greiner, O. Mandel, T. W. Hänsch, and I. Bloch, Collapse and revival of the matter wave field of a Bose–Einstein condensate, Nature (London) **419**, 51 (2002).
[2] M. Cetina, M. Jag, R. S. Lous, I. Fritsche, J. T. M. Walraven, R. Grimm, J. Levinsen, M. M. Parish, R. Schmidt, M. Knap, and E. Demler, Ultrafast many-body interferometry of impurities coupled to a Fermi sea, Science **354**, 96 (2016).
[3] H. Bernien, S. Schwartz, A. Keesling, H. Levine, A. Omran, H. Pichler, S. Choi, A. S. Zibrov, M. Endres, M. Greiner, V. Vuletić, and M. D. Lukin, Probing many-body dynamics on a 51-atom quantum simulator, Nature (London) **551**, 579 (2017).
[4] M. Prüfer, P. Kunkel, H. Strobel, S. Lannig, D. Linnemann, C.-M. Schmied, J. Berges, T. Gasenzer, and M. K. Oberthaler, Observation of universal dynamics in a spinor Bose gas far from equilibrium, Nature (London) **563**, 217 (2018).
[5] S. Erne, R. Bücker, T. Gasenzer, J. Berges, and J. Schmiedmayer, Universal dynamics in an isolated one-dimensional Bose gas far from equilibrium, Nature (London) **563**, 225 (2018).
[6] R. Senaratne, S. V. Rajagopal, T. Shimasaki, P. E. Dotti, K. M. Fujiwara, K. Singh, Z. A. Geiger, and D. M. Weld, Quantum simulation of ultrafast dynamics using trapped ultracold atoms, Nat. Commun. **9**, 2065 (2018).
[7] M. G. Skou, T. G. Skov, N. B. Jørgensen, K. K. Nielsen, A. Camacho-Guardian, T. Pohl, G. M. Bruun, and J. J. Arlt, Non-equilibrium quantum dynamics and formation of the Bose polaron, Nat. Phys. **17**, 731 (2021).
[8] J. Etrych, G. Martirosyan, A. Cao, C. J. Ho, Z. Hadzibabic, and C. Eigen, Universal quantum dynamics of Bose polarons, Phys. Rev. X **15**, 021070 (2025).
[9] F. J. Vivanco, A. Schuckert, S. Huang, G. L. Schumacher, G. G. T. Assumpção, Y. Ji, J. Chen, M. Knap, and N. Navon, The strongly driven Fermi polaron, Nat. Phys. **21**, 564 (2025).
[10] P. Makotyn, C. E. Klauss, D. L. Goldberger, E. A. Cornell, and D. S. Jin, Universal dynamics of a degenerate unitary Bose gas, Nat. Phys. **10**, 116 (2014).
[11] R. J. Fletcher, R. Lopes, J. Man, N. Navon, R. P. Smith, M. W. Zwierlein, and Z. Hadzibabic, Two- and three-body contacts in the unitary Bose gas, Science **355**, 377 (2017).
[12] C. Eigen, J. A. P. Glidden, R. Lopes, N. Navon, Z. Hadzibabic, and R. P. Smith, Universal scaling laws in the dynamics of a homogeneous unitary Bose gas, Phys. Rev. Lett. **119**, 250404 (2017).
[13] C. E. Klauss, X. Xie, C. Lopez-Abadia, J. P. D'Incao, Z. Hadzibabic, D. S. Jin, and E. A. Cornell, Observation of Efimov molecules created from a resonantly interacting Bose gas, Phys. Rev. Lett. **119**, 143401 (2017).

[14] C. Eigen, J. A. P. Glidden, R. Lopes, E. A. Cornell, R. P. Smith, and Z. Hadzibabic, Universal prethermal dynamics of Bose gases quenched to unitarity, Nature (London) **563**, 221 (2018).
[15] Z. Zhang, S. Nagata, K.-X. Yao, and C. Chin, Many-body chemical reactions in a quantum degenerate gas, Nat. Phys. **19**, 1466 (2023).
[16] S. S. Natu and E. J. Mueller, Dynamics of correlations in a dilute Bose gas following an interaction quench, Phys. Rev. A **87**, 053607 (2013).
[17] A. G. Sykes, J. P. Corson, J. P. D'Incao, A. P. Koller, C. H. Greene, A. M. Rey, K. R. A. Hazzard, and J. L. Bohn, Quenching to unitarity: Quantum dynamics in a three-dimensional Bose gas, Phys. Rev. A **89**, 021601(R) (2014).
[18] J. P. Corson and J. L. Bohn, Bound-state signatures in quenched Bose-Einstein condensates, Phys. Rev. A **91**, 013616 (2015).
[19] J. P. D'Incao, J. Wang, and V. E. Colussi, Efimov physics in quenched unitary Bose gases, Phys. Rev. Lett. **121**, 023401 (2018).
[20] A. Muñoz de las Heras, M. M. Parish, and F. M. Marchetti, Early-time dynamics of Bose gases quenched into the strongly interacting regime, Phys. Rev. A **99**, 023623 2019).
[21] V. E. Colussi, H. Kurkjian, M. Van Regemortel, S. Musolino, J. van de Kraats, M. Wouters, and S. J. J. M. F. Kokkelmans, Cumulant theory of the unitary Bose gas: Prethermal and Efimovian dynamics, Phys. Rev. A **102**, 063314 (2020).
[22] M. Sun, P. Zhang, and H. Zhai, High temperature virial expansion to universal quench dynamics, Phys. Rev. Lett. **125**, 110404 (2020).
[23] C. Gao, M. Sun, P. Zhang, and H. Zhai, Universal dynamics of a degenerate Bose gas quenched to unitarity, Phys. Rev. Lett. **124**, 040403 (2020).
[24] R. Qi, Z. Shi, and H. Zhai, Maximum energy growth rate in dilute quantum gases, Phys. Rev. Lett. **126**, 240401 (2021).
[25] D. J. M. Ahmed-Braun, S. Musolino, V. E. Colussi, and S. J. J. M. F. Kokkelmans, Evolution of the unitary Bose gas for broad to narrow Feshbach resonances, Phys. Rev. A **106**, 013315 (2022).
[26] X. Yang and R. Zhang, Quench dynamics of thermal Bose gases across wide and narrow Feshbach resonances, Phys. Rev. A **107**, 063310 (2023).
[27] J.-N. Cui, Z. Zhou, and M. Sun, Universal dynamic scaling and Contact dynamics in quenched quantum gases, Front. Phys. **19**, 22201 (2024).
[28] J. van de Kraats, D. J. M. Ahmed-Braun, V. E. Colussi, and S. J. J. M. F. Kokkelmans, Resonance triplet dynamics in the quenched unitary Bose gas, Phys. Rev. Res. **6**, L012056 (2024).
[29] Z. Wang, K. Wang, Z. Zhang, S. Nagata, C. Chin, and K. Levin, Stability and dynamics of atom-molecule superfluids near a narrow Feshbach resonance, Phys. Rev. A **110**, 013306 (2024).
[30] K. Wang, Z. Zhang, S. Nagata, Z. Wang, and K. Levin, Universal coherent atom-molecule oscillations in the dynamics of the unitary Bose gas near a narrow Feshbach resonance, Phys. Rev. Res. **7**, L012025 (2025).
[31] S. Tan, Large momentum part of a strongly correlated Fermi gas, Ann. Phys. (Amsterdam) **323**, 2971 (2008).
[32] S. Tan, Energetics of a strongly correlated Fermi gas, Ann. Phys. (Amsterdam) **323**, 2952 (2008).
[33] S. Tan, Generalized virial theorem and pressure relation for a strongly correlated Fermi gas, Ann. Phys. (Amsterdam) **323**, 2987 (2008).
[34] E. Braaten and L. Platter, Exact relations for a strongly interacting Fermi gas from the operator product expansion, Phys. Rev. Lett. **100**, 205301 (2008).
[35] S. Zhang and A. J. Leggett, Universal properties of the ultracold Fermi gas, Phys. Rev. A **79**, 023601 (2009).
[36] E. Braaten, D. Kang, and L. Platter, Universal relations for identical bosons from three-body physics, Phys. Rev. Lett. **106**, 153005 (2011).
[37] F. Werner and Y. Castin, General relations for quantum gases in two and three dimensions. II. Bosons and mixtures, Phys. Rev. A **86**, 053633 (2012).
[38] E. Braaten, Universal relations for fermions with large scattering length, in *The BCS-BEC Crossover and the Unitary Fermi Gas*, Lecture Notes in Physics Vol. 836, edited by W. Zwerger (Springer, New York, 2012), pp. 193–231.
[39] R. Weiss, B. Bazak, and N. Barnea, Nuclear neutron-proton contact and the photoabsorption cross section, Phys. Rev. Lett. **114**, 012501 (2015).
[40] R. Weiss, R. Cruz-Torres, N. Barnea, E. Piasetzky, and O. Hen, The nuclear contacts and short range correlations in nuclei, Phys. Lett. B **780**, 211 (2018).
[41] A. Schmidt *et al.* (The CLAS Collaboration). Probing the core of the strong nuclear interaction, Nature (London) **578**, 540 (2020).
[42] R. Cruz-Torres, D. Lonardoni, R. Weiss, M. Piarulli, N. Barnea, D. W. Higinbotham, E. Piasetzky, A. Schmidt, L. B. Weinstein, R. B. Wiringa, and O. Hen, Many-body factorization and position–momentum equivalence of nuclear short-range correlations, Nat. Phys. **17**, 306 (2021).
[43] R. J. Wild, P. Makotyn, J. M. Pino, E. A. Cornell, and D. S. Jin, Measurements of Tan's contact in an atomic Bose-Einstein condensate, Phys. Rev. Lett. **108**, 145305 (2012).
[44] Y.-Q. Zou, B. Bakkali-Hassani, C. Maury, É. Le Cerf, S. Nascimbene, J. Dalibard, and J. Beugnon, Tan's two-body contact across the superfluid transition of a planar Bose gas, Nat. Commun. **12**, 760 (2021).
[45] D. H. Smith, E. Braaten, D. Kang, and L. Platter, Two-body and three-body contacts for identical bosons near unitarity, Phys. Rev. Lett. **112**, 110402 (2014).
[46] G. B. Partridge, K. E. Strecker, R. I. Kamar, M. W. Jack, and R. G. Hulet, Molecular probe of pairing in the BEC-BCS crossover, Phys. Rev. Lett. **95**, 020404 (2005).
[47] F. Werner, L. Tarruell, and Y. Castin, Number of closed-channel molecules in the BEC-BCS crossover, Eur. Phys. J. B **68**, 401 (2009).
[48] J. Wang, X.-J. Liu, and H. Hu, Photoexcitation measurement of Tan's contact for a strongly interacting Fermi gas, Phys. Rev. A **104**, 063309 (2021).

[49] M. Jäger and J. H. Denschlag, Precise photoexcitation measurement of Tan's contact in the entire BCS-BEC crossover, Phys. Rev. Lett. **132**, 263401 (2024).
[50] C. Chin, R. Grimm, P. S. Julienne, and E. Tiesinga, Feshbach resonances in ultracold gases, Rev. Mod. Phys. **82**, 1225 (2010).
[51] D. S. Petrov, Three-boson problem near a narrow Feshbach resonance, Phys. Rev. Lett. **93**, 143201 (2004).
[52] E. Braaten, D. Kang, and L. Platter, Universal relations for a strongly interacting Fermi gas near a Feshbach resonance, Phys. Rev. A **78**, 053606 (2008).
[53] L. Pricoupenko, Many bosons in a narrow magnetic Feshbach resonance, Phys. Rev. Lett. **110**, 180402 (2013).
[54] A. Schwenk and C. J. Pethick, Resonant Fermi gases with a large effective range, Phys. Rev. Lett. **95**, 160401 (2005).
[55] J. Carlson, S. Gandolfi, and A. Gezerlis, Quantum Monte Carlo approaches to nuclear and atomic physics, Prog. Theor. Exp. Phys. **2012**, 01A209 (2012).
[56] L. Platter and D. T. Son, Non-Efimovian two-neutron halos with an *s*-wave core-neutron resonance, arXiv:2507.19171.
[57] J. H. Becher, S. Baier, K. Aikawa, M. Lepers, J.-F. Wyart, O. Dulieu, and F. Ferlaino, Anisotropic polarizability of erbium atoms, Phys. Rev. A **97**, 012509 (2018).
[58] T. Chalopin, V. Makhalov, C. Bouazza, A. Evrard, A. Barker, M. Lepers, J.-F. Wyart, O. Dulieu, J. Dalibard, R. Lopes, and S. Nascimbene, Anisotropic light shift and magic polarization of the intercombination line of dysprosium atoms in a far-detuned dipole trap, Phys. Rev. A **98**, 040502(R) (2018).
[59] M. Kreyer, J. H. Han, C. Ravensbergen, V. Corre, E. Soave, E. Kirilov, and R. Grimm, Measurement of the dynamic polarizability of Dy atoms near the 626-nm intercombination line, Phys. Rev. A **104**, 033106 (2021).
[60] A similar mechanism has been used in a Li-K mixture [2]. In that case, the light shift also acts in the open channel, and special care is required to avoid modifications of the trapping frequencies.
[61] E. A. Donley, N. R. Claussen, S. T. Thompson, and C. E. Wieman, Atom–molecule coherence in a Bose–Einstein condensate, Nature (London) **417**, 529 (2002).
[62] N. R. Claussen, S. J. J. M. F. Kokkelmans, S. T. Thompson, E. A. Donley, E. Hodby, and C. E. Wieman, Very-high-precision bound-state spectroscopy near a ^{85}Rb Feshbach resonance, Phys. Rev. A **67**, 060701(R) (2003).
[63] R. Elbaz, Y. Yudkin, P. Giannakeas, J.-M. Rost, C. H. Greene, and L. Khaykovich, Observation of coherent oscillations in the association of dimers from a thermal gas of ultracold atoms, Phys. Rev. A **107**, L031304 (2023).
[64] M. Lecomte, A. Journeaux, J. Veschambre, J. Dalibard, and R. Lopes, Production and stabilization of a spin mixture of ultracold dipolar Bose gases, Phys. Rev. Lett. **134**, 013402 (2025).
[65] D. M. Bauer, M. Lettner, C. Vo, G. Rempe, and S. Dürr, Control of a magnetic Feshbach resonance with laser light, Nat. Phys. **5**, 339 (2009).
[66] A. Jagannathan, N. Arunkumar, J. A. Joseph, and J. E. Thomas, Optical control of magnetic Feshbach resonances by closed-channel electromagnetically induced transparency, Phys. Rev. Lett. **116**, 075301 (2016).
[67] For comparison, this is an order of magnitude faster than the state-of-the-art magnetic field quench time for broad FFRs [68].
[68] A. Kell, M. Link, M. Breyer, A. Hoffmann, M. Köhl, and K. Gao, A compact and fast magnetic coil for the manipulation of quantum gases with Feshbach resonances, Rev. Sci. Instrum. **92**, 093202 (2021).
[69] See Supplemental Material at http://link.aps.org/supplemental/10.1103/prf8-3q27 for more details on density dependence of losses, cycling procedure, extracting L_2 in a thermal gas with evolving temperature, temperature dependence of the resonance loss feature, fitting procedure to extract $R^\star$ and Γ_b, evolution of L_2 as a function of t_{on} and t_{off}, derivation of the dynamical equation for the closed-channel amplitude, single-quench evolution of $\mathcal{C}_2(t)$, and Floquet analysis, which includes Refs. [70,71].
[70] B. S. Rem, A. T. Grier, I. Ferrier-Barbut, U. Eismann, T. Langen, N. Navon, L. Khaykovich, F. Werner, D. S. Petrov, F. Chevy, and C. Salomon, Lifetime of the Bose gas with resonant interactions, Phys. Rev. Lett. **110**, 163202 (2013).
[71] A. Pricoupenko and D. S. Petrov, Three-body interaction near a narrow two-body zero crossing, Phys. Rev. A **100**, 042707 (2019).
[72] Y. Castin and F. Werner, The unitary gas and its symmetry properties, in *The BCS-BEC Crossover and the Unitary Fermi Gas*, Lecture Notes In Physics Vol. 836, edited by W. Zwerger (Springer, New York, 2012), p. 127.
[73] There is a factor 2 difference compared to the fermionic case considered in Refs. [47,72], because for fermions, $\mathcal{C}_2$ is defined as the prefactor of the $1/k^4$ tail of the *spin-resolved* momentum distribution.
[74] Here, we assume that n is time-independent as it enters in our theoretical analysis only through the density of pairs $n^2/2$ and evolves on a much longer timescale than the buildup dynamics we are interested in.
[75] M. Lecomte, A. Journeaux, L. Renaud, J. Dalibard, and R. Lopes, Loss features in ultracold ^{162}Dy gases: Two- versus three-body processes, Phys. Rev. A **109**, 023319 (2024).
[76] A. G. Sykes, H. Landa, and D. S. Petrov, Two-and three-body problem with Floquet-driven zero-range interactions, Phys. Rev. A **95**, 062705 (2017).
[77] T. Maier, H. Kadau, M. Schmitt, M. Wenzel, I. Ferrier-Barbut, T. Pfau, A. Frisch, S. Baier, K. Aikawa, L. Chomaz, M. J. Mark, F. Ferlaino, C. Makrides, E. Tiesinga, A. Petrov, and S. Kotochigova, Emergence of chaotic scattering in ultracold Er and Dy, Phys. Rev. X **5**, 041029 (2015).
[78] Dataset for the manuscript "Two-Body Contact Dynamics in a Bose Gas near a Fano-Feshbach Resonance," 10.5281/zenodo.18433399.
[79] L. Zhou and X. Cui, Effective scattering and Efimov physics in the presence of two-body dissipation, Phys. Rev. Res. **3**, 043225 (2021).

End Matter

Determination of Γ_b and $R^\star$ from spectroscopy of the dimer energy—To determine the closed-channel dimer energy as a function of magnetic field, we apply the SLS beam with a temporal intensity profile $I(t) = I_0 + I_1 \sin^2(\Omega t/2)$. For half of the data we use $I_0 = 0$ and $I_1 = 1.0\ \mu\mathrm{W}/\mu\mathrm{m}^2$ (SLS off in Fig. 5), which places the FFR pole at $B_0 \approx 5.15$ G. For the other half we set $I_0 = 15\ \mu\mathrm{W}/\mu\mathrm{m}^2$ and $I_1 = 1.5\ \mu\mathrm{W}/\mu\mathrm{m}^2$ (SLS on in Fig. 5), shifting the pole to $B_1 \approx 5.07$ G. In both cases the average intensity is $I_0 + I_1/2$. We then scan the frequency Ω around the molecular binding energy and observe resonant atom loss when $\hbar\Omega$ matches the real part of the closed-channel binding energy, signaling the formation of weakly bound molecules that subsequently decay (see Fig. 5, top panel). The extracted binding energies as a function of magnetic field are shown in Fig. 5 (bottom panel).

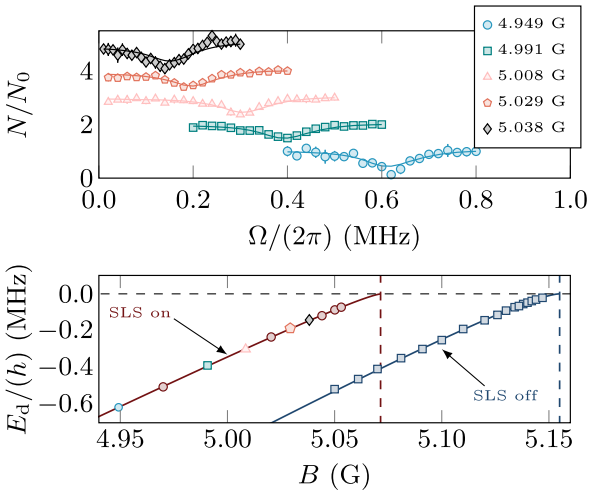

FIG. 5. Determination of the narrow Fano-Feshbach resonance properties. Top: resonance spectra of atom losses as a function of the modulation frequency Ω for various magnetic fields (see legend). For visual clarity, the different curves are vertically offset by consecutive integer values. The solid lines are fits to the data using Eq. (4). Bottom: resonance frequency as a function of magnetic field, for $I_0 = 0$ (SLS off) and $I_0 = 15\ \mu\mathrm{W}/\mu\mathrm{m}^2$ (SLS on). The solid line shows the expected dressed Feshbach dimer energy dependence on magnetic field with the parameters listed in Table I.

The only differences between the two datasets are the effective resonance position, determined by the SLS beam, and the inverse lifetime of the molecular state, Γ_b, which increases with SLS intensity. The value of Γ_b^{off} is much smaller than Γ_b^{on}, yet remains finite. Its value is likely set by photodissociation from the infrared trapping lasers. We observed that Γ_b^{off} remained unchanged for I_1 up to $2.0\ \mu\mathrm{W}/\mu\mathrm{m}^2$ (a factor of 2 increase), indicating that the contribution from the residual SLS average intensity, $I_1/2$, is negligible in this regime.

The best-fit parameters characterizing the resonance spectra are reported in Table I. The line shown in Fig. 5 corresponds to the following expression for the real part of the dressed Feshbach dimer energy [79]:

$$\mathrm{Re}(E_d) = -\frac{\hbar^2}{4mR^{\star 2}}\left(\sqrt{1 + 4R^\star/a'} - 1\right)^2, \tag{A1}$$

with

$$a' = -\frac{\hbar^2}{mR^\star \delta\mu (B - B_{\mathrm{res}})}, \tag{A2}$$

where B_{res} is the position of the FFR; $B_{\mathrm{res}} = B_0$ (resp. $B_{\mathrm{res}} = B_1$) when the SLS is off (resp. on).

TABLE I. Values of the FFR position, B_{res}, differential magnetic moment, $\delta\mu$, and $R^\star$ in the presence and absence of the spin-dependent light shift.

	$I_0 = 0$ (SLS off)	$I_0 \neq 0$ (SLS on)
$\delta\mu(\mu_B)$	4.35 (16)	4.15 (18)
B_{res}(G)	5.154 (2)	5.073 (2)
$R^\star(\ell_{\mathrm{vdW}})$	10.2 (1.8)	10.8 (2.1)
$\Gamma_b/(2\pi)$ (kHz)	20 (10)	112 (30)